

# Simulation and Reduction of Speckle-induced Uncertainty in Laser Triangulation Sensors

Ernst Csencsics\*, Johannes Schlarp\*, Tobias Glaser, Tobias Wolf and Georg Schitter, *Senior Member, IEEE*

*Automation and Control Institute (ACIN), Technische Universität Wien*

*Vienna, Austria*

csencsics@acin.tuwien.ac.at

**Abstract**—Laser triangulation sensors are one of the most commonly used optical sensors in dimensional metrology and quality control. This paper presents a method for simulating the laser speckle-induced measurement uncertainty, representing a major performance limitation of these sensors, as well as a method for reducing the influence of speckle on the achievable accuracy. To investigate the relation between triangulation angle and the resulting speckle-induced uncertainty, simulations are performed for three sensor geometries, revealing that a larger angle results not only in a smaller measurement range but also in a reduced influence of laser speckles and a smaller uncertainty. The accuracy of the simulation method is validated by measurements conducted with an experimental setup, demonstrating good agreement between the measured and simulated uncertainty values. To reduce the impact of speckles on the measurement accuracy, a diffuser mechanism is integrated into the optical path, reducing the resulting speckle-induced measurement uncertainty by up to 63%.

**Index Terms**—laser speckle, triangulation sensor, measurement uncertainty, simulation tool, speckle reduction

## I. INTRODUCTION

Quality requirements in the manufacturing industry are ever increasing, such that robust high precision measurement systems are more and more required [1]. To enable real-time control of manufacturing process and continuous quality control, measurements should be performed directly in the production line to detect errors at an early stage [2], without decreasing the throughput [3]. State of the art sensor systems for these applications are mostly based on optical principles, like laser triangulation, the confocal chromatic principle or white light interferometry [4]. Compared to tactile sensors they provide shorter measurement times, higher throughput and they are based on non-contacting measurement principles, minimizing the physical interaction with the sample [5].

Among available optical measurement systems, laser triangulation sensors are one of the most commonly used ones in quality control and dimensional metrology, due to their high resolution of down to 30 nm and their large measurement range of up to 1 m [6]. The measurement principle is robust in handling varying reflection properties of the sample and illumination conditions, since intensity is typically adjusted

according to the sample surface property and optical filters are used to reduce influence of external illumination. The principle enables measurements on specular and diffuse reflective surfaces and is based on a rather simple design [6].

The achievable accuracy and uncertainty of a laser triangulation sensor is to a major extent restrained by laser speckle noise on the detector [7], [8]. With an optically rough surface being illuminated by coherent light, each illuminated spot on the micro-structured surface represents an individual scatterer, scattering the incoming light randomly in direction, amplitude and phase [9]. A superposition of the scattered waves on the detector results in a grainy pattern of bright and dark spots, affecting the calculation of the center of gravity of the measurement spot in a stochastic manner and adding uncertainty to the measurement. This influence of speckle on the resulting uncertainty has been experimentally studied and mathematically modeled for microscopic measurements on various technical surfaces [10] in the past. Further also a framework for uncertainty propagation in laser line sensors [11] and a sensor-realistic simulation approach for the evaluation of optical measurement systems, both relying on rather complex mathematical models, have been developed [12]. In terms of reducing speckle effects on the resulting measurement uncertainty, an approach with a dual-view triangulation sensor has been proposed, which is, however, limited to certain surface profiles [13].

The contribution of this paper is (i) an accurate method for simulating the effects of speckle on the uncertainty of a laser triangulation sensor, integrating the stochastic nature of laser speckles with the deterministic properties of ray tracing simulations, (ii) its experimental validation and (iii) a method for reducing the effects on the resulting uncertainty. The integrated simulation method, presented in Section II, enables the consideration of various optical elements, a fast modification for various sensor geometries, the efficient consideration of geometric uncertainty sources and provides several simulation outputs, such as sensor characteristic or uncertainty. In Section III a parametric study on the relation of triangulation angle and uncertainty is conducted and the experimental setup with integrated speckle reduction mechanism is designed. Section IV compares the experimental and simulation results and Section V concludes the paper.

\* ) Authors contributed equally to this publication. All authors are with the Christian Doppler Laboratory for Precision Engineering for Automated In-Line Metrology, Automation and Control Institute (ACIN), Technische Universität Wien, 1040 Vienna.

## II. LASER SPECKLE SIMULATION

The simulation method integrates the stochastic nature of laser speckles with the deterministic properties of the ray tracing method in order to make it applicable for the design of optical sensors [14]. Starting with the definition of the system geometry the location, orientation and size of the laser source, the target surface, the detector (with number and size of pixels) and the imaging as well as the focusing lens are defined. The laser spot on the target is approximated by  $N_1$  point sources, which are laterally distributed within the spot diameter and randomly distributed within the expected surface roughness of the target material in z-direction. The related intensities of the point sources are normally distributed to resemble a Gaussian beam intensity profile (see Fig. 1).

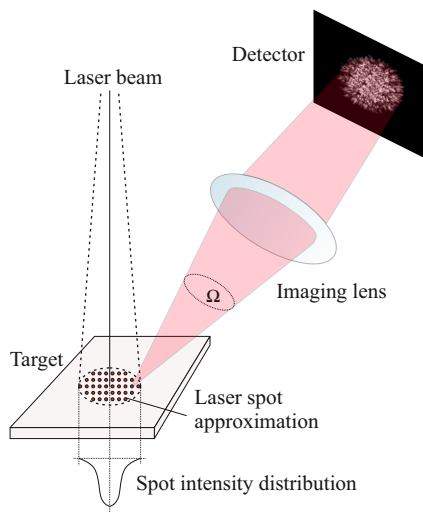


Fig. 1. Simulation environment. The laser spot on the target is approximated by  $N_1$  point sources with normally distributed intensity profile and height distribution according to the roughness of the surface. Ray tracing of  $N_2$  rays beaming out under solid angle  $\Omega$  is performed for each point for calculation of the phase image on the detector.

To determine the intensity profile of the  $N_1$  point sources on the detector,  $N_2$  rays are used, which beam out equally distributed over a pre-set solid angle  $\Omega$ , which is matched to the size of the imaging lens. Using the ray tracing, each of the emerging rays is propagated through the imaging lens towards the detector. All rays not intersecting with the pre-defined detector area, are discarded for the further considerations. With the known laser wavelength and the individual optical path lengths, the phase of each ray at the intersection point with the detector can be calculated. To calculate possibly missing phase values, grid data interpolation with a meshgrid according to the pixel size is employed. This sequence is repeated for all  $N_1$  point sources. The spot image on the detector including the resulting laser speckle is then calculated by complex superposition of the intensity and phase image matrices of the individual point sources.

An out-of-plane target displacement is simulated via manipulating the absolute laser point source positions and the solid angle  $\Omega$  according to the defined geometry. The illuminated spot area is varied according to the parameters of the focusing lens, such that point sources leaving the spot area are set invalid. After adapting the point source positions and the illuminated area on the surface, which keeps its Gaussian intensity distribution, a new detector image including speckle is generated according to the previous procedure. Based on the respective spot image on the detector, the center of gravity (CoG) is calculated as measure for the distance to the target, which is affected by the uncertainty introduced by the laser speckle. The formation of a representative speckle pattern requires a minimum number of point sources  $N_1$  for approximating the laser spot on the target, which should, however, be kept as small as possible for the sake of computational efficiency. Setting the number of point sources to  $N_1 = 100$  leads to a good approximation of a fully developed speckle pattern for the given case. The basic implementation of the simulation method is done in *MATLAB* (MathWorks Inc., MA, USA) using the *Optometrika* library [15], which provides basic ray tracing functionality together with a number of optical elements.

## III. TRIANGULATION SENSOR GEOMETRY AND SPECKLE-INDUCED UNCERTAINTY

### A. Triangulation Geometry

Triangulation sensors typically consist out of a laser diode, emitting the laser beam which is focused onto the sample via the focusing lens. Light hitting the sample is diffusely scattered at the point where the beam irradiates the surface. As shown in Fig. 2, the imaging lens projects this scattered light spot onto the detector. The lateral position of the projected spot on the detector provides an accurate measure for the distance between sensor and sample. To precisely obtain this distance, an equally sharp projection of the light spot onto the detector is required over the entire measurement range [5]. In order to meet this requirement, the components of the triangulation sensor are aligned according to the Scheimpflug condition, which is a generalized form of the thin-lens equation for non parallel planes [16]. This Scheimpflug condition is satisfied, if the object, (imaging) lens and image plane intersect in a single line (see intersection line in Fig. 2) [17].

The relation between the position of the laser spot, or more precisely its CoG, on the detector  $\Delta d$  and the distance between sensor and sample  $d$ , which is shown in Fig. 2, is given by

$$\Delta d = d \cdot \frac{\sqrt{1 + \left(m_L + \frac{u_0}{f}\right)^2} \cdot m_L f}{d(m_L - \frac{u_0}{f}) + \sqrt{1 + m_L^2(2u_0 - m_L f - \frac{u_0^2}{m_L f})}} \quad (1)$$

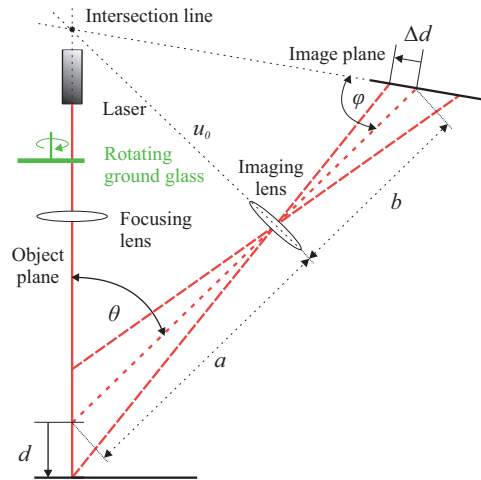


Fig. 2. Measurement principle of triangulation sensor. The sensor is composed of a laser source, a focusing lens, an imaging lens and detector, which are aligned according to the Scheimpflug condition. The sensitivity of the sensor is mainly determined via the triangulation angle  $\theta$ . A rotating ground glass is added to reduce the formation of speckle on the detector.

with  $\theta$  the triangulation angle between object plane and optical axis of the imaging lens and the resulting constant  $m_L = \tan(\theta)$ ,  $f$  the focal length of the imaging lens and  $u_0$  the distance between center point of the lens and intersection line. From this relation it is apparent that the resulting sensitivity  $k(d)$  of the triangulation sensor is non-uniform and decreases with increasing values of  $d$ .

The setup schematic (see Fig. 2) also includes a rotating ground glass as diffuser mechanism, which is used to reduce the formation of speckle on the detector and will be revised in Section III-C.

### B. Speckle-induced Uncertainty Simulation

In order to investigate the capabilities of the simulation method to assess arbitrary triangulation sensor designs, the sensor characteristic, the speckle-induced uncertainty of the resulting CoG displacement  $\Delta d$  on the detector are simulated for three sensor assemblies. Additionally the uncertainty of the actual distance measurement, obtained via CoG displacement and the local sensitivity (see (1)) is calculated. All three assemblies are composed of the same optical elements including a focusing lens (bi-convex, focal length 50 mm, aperture 25.4 mm), imaging lens (focal length  $f = 16$  mm, aperture 6.4 mm) and a detector (640 x 480 pixels with a size of  $1.85 \mu\text{m}$ ). All assemblies are designed for the same distance  $u_0 = 95$  mm and triangulation angles of  $\theta = \{16^\circ, 33^\circ, 66^\circ\}$ . The diffuser mechanism is not considered in the simulation. The remaining geometric dimensions of

each setup can according to Fig. 2 be calculated via:

$$\begin{aligned} a &= \tan(\theta) \cdot u_0 \\ b &= a \cdot f / (a - f) \\ \phi &= \tan^{-1}(u_0/b) \end{aligned} \quad (2)$$

In Fig. 3 the simulation results are depicted for all three sensor assemblies. The resulting sensitivities are shown in Fig. 3 and amount around the center of the measurement range to 22.15 pixel/mm ( $41 \mu\text{m}/\text{mm}$ ), 38.87 pixel/mm ( $71.9 \mu\text{m}/\text{mm}$ ) and 63.42 pixel/mm ( $117.3 \mu\text{m}/\text{mm}$ ) for the three angles, respectively, scaling approximately with the ratio of the tangent values. Given the higher sensitivity of the larger triangulation angles and the fixed detector size for all setups, the measurement range decreases accordingly for larger values of  $\theta$ .

To obtain a measure for the speckle-induced uncertainty of the CoG displacement  $\Delta d$  as a function of the triangulation angle and the distance  $d$ , 50 simulations with randomly varying spot locations, approximating the spot on the target (see Section II), are performed at distance steps of 1 mm for each of the three assemblies and the standard deviation (STD) of  $\Delta d$  is calculated. The results depicted in Fig. 3(b) show an almost symmetric STD CoG value distribution for the two smaller triangulation angles with the smallest angle giving the slightly higher uncertainty values. The largest angle shows an almost constant uncertainty distribution over the target distance with a significantly smaller average uncertainty value. Using the calculated STD values of  $\Delta d$  and the local sensitivity of the sensor  $k(d)$  (see Fig. 3(a)), the STD of the actually measured distance can be calculated as measure of the resulting measurement uncertainty. Fig. 3c shows the resulting uncertainty values with mean values of 0.0187 mm, 0.0392 mm and 0.068 mm for the angles of  $66^\circ$ ,  $33^\circ$  and  $16^\circ$ , respectively. Considering the increased measurement range with smaller angle  $\theta$  the increase in measurement uncertainty is not surprising with the ratios of speckle-induced uncertainty to range staying almost between 0.2% and 0.26%. However, the assembly with  $\theta = 66^\circ$ , shows with 0.2% the smallest ratio, suggesting a reduced influence of speckle on the resulting uncertainty with larger triangulation angles.

### C. Experimental Setup

The experimental setup of the triangulation sensor is depicted in Fig. 4 and is composed of a CMOS sensor (DMM 37UX266-ML, Imaging Source GmbH, Germany; 640 x 480 pixel with a size of  $1.85 \mu\text{m}$ ) as detector and a laser source (LDM635/1LJ, Roithner Lasertechnik GmbH, Austria), which is focused on the target via a bi-convex lens (N-BK7 LB1471, Thorlabs Inc.) with a focal length of 50 mm. The setup is designed for a measurement range of  $\pm 10$  mm with the minimum spot diameter placed in the center of the measuring range a triangulation angle of  $\theta = 33^\circ$  and a distance  $u_0 = 95$  mm. The imaging lens (V-4316-2.5, Marshall Electronics Inc.;  $f = 16$  mm) is used to obtain the image of the measurement spot on the CMOS detector and

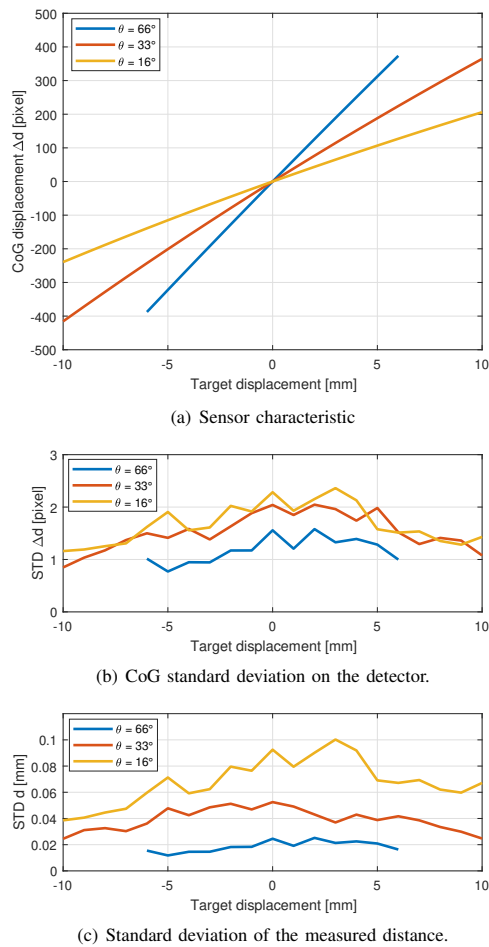


Fig. 3. Simulated sensor characteristic and speckle-induced uncertainty. (a) shows the simulated sensor characteristic for all three geometric configurations. (b) depicts the CoG standard deviation on the detector of 50 simulations at each target displacement and (c) the resulting standard deviation of the measured distance, derived via the sensor characteristic.

is placed in a distance of  $a = 141$  mm from the center of the measurement range. The CMOS sensor is mounted in a distance of  $b = 14.4$  mm from the imaging lens and is rotated by  $\varphi = 81^\circ$ .

The diffuser mechanism is implemented via a NEMA17 stepper motor with a ground glass (DG20-1500, Thorlabs Inc.) mounted on its shaft, which is installed between the bi-convex lens and the laser source. This locates the diffuser in the part of the optical path in which the laser beam is still collimated, avoiding a potential additional uncertainty of the measurement spot location due to a lateral displacement of the focus point on the sample caused by the diffuser motion. The stepper motor is speed-controlled with an Arduino UNO R3 micro-controller via a stepper driver module (A4988, Allegra

Microsystems LLC) (see [18]). The aperture is inserted to reduce the influence of stray light from the diffuser.

In order to enable out-of-plane as well as in-plane displacement of the target, which is a machined aluminum part, it is placed on two stacked linear stages. For accurate displacement of the target in the measurement direction (out-of-plane) a position-controlled linear stage (VT-80 62309120, Physik Instrumente GmbH, Germany) with a resolution of 500 nm and a range of 80 mm is used, covering the entire measuring range of the sensor assembly. For in-plane displacement a piezoelectrically actuated and position controlled linear translation stage (ELL17 / M, Thorlabs Inc.) with a range of 28 mm is used, in order to enable experiments with varying speckle distributions in the same target distance.

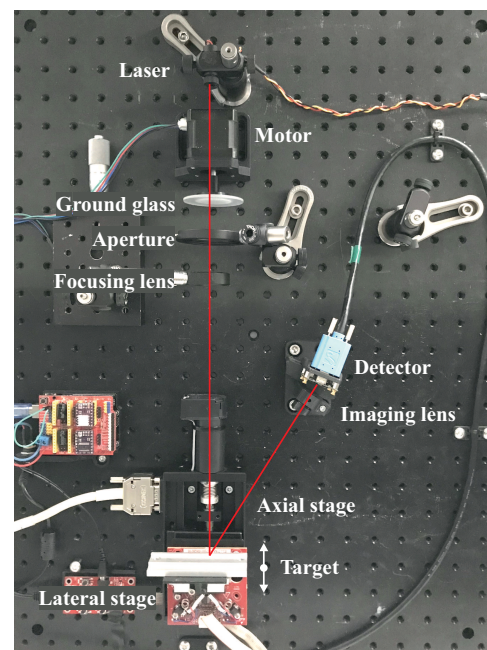


Fig. 4. Experimental setup. The laser of the source passes through the ground glass, which is rotated by a motor, an aperture and the focusing lens before hitting the target. The spot on the target is via the imaging lens imaged on the detector. Linear stages are used to displace the target in- and out-of-plane.

#### IV. EXPERIMENTAL RESULTS

To validate the performance of the simulation method and the effectiveness of the diffuser mechanism, the resulting measurement uncertainty for the designed experimental setup with and without diffuser is evaluated for 1 mm steps over the entire measurement range of  $\pm 10$  mm. At each displacement 50 measurements are obtained with the target being laterally displaced before each measurement in order to obtain uncorrelated and sufficiently varying speckle patterns on the detector.

In Fig. 5(a) the simulated and measured sensor characteristic are shown, as well as the error of both characteristics with

respect to the analytic solution based on the nominal geometric dimensions of the assembly. The simulated characteristic is obtained by taking the mean value of 50 simulations at each target displacement in order to minimize the influence of speckle-induced uncertainty. It can be seen that both errors stay within half a pixel of the detector throughout the entire measurement range, indicating the good agreement of all three sensor characteristics and minimal mounting tolerances of the experimental setup.

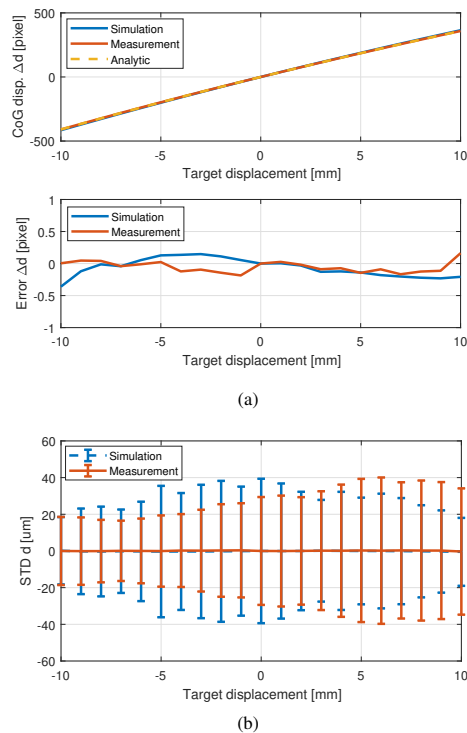


Fig. 5. Comparison of simulated and measured sensor characteristic and measurement uncertainty. (a) shows the simulated, measured and analytically calculated characteristic as well as the mean error in terms of CoG location on the detector with respect to the analytic value. (b) is a graph for the standard deviation of 50 simulation and measurement results at each displacement. The uncertainty increases by about a factor of two from start ( $z = -10$  mm) till end ( $z = 10$  mm) of the measurement range.

To compare the simulation result in terms of speckle-induced uncertainty, the graph in Fig. 5(b), shows the standard deviation of 50 simulations (blue) and measurements (red) at each target displacement. It can be seen that the results match well, showing only small deviations over the majority of the measurement range. The simulation shows a rather equal uncertainty distribution over the measurement range of about  $30 \mu\text{m}$ , while the measured uncertainty gradually increases towards larger displacements, and doubles from about  $20 \mu\text{m}$  to about  $40 \mu\text{m}$ . At smaller distances the simulation thus tends to overestimate the resulting uncertainty as compared to the measurement, while it tends to underestimate it towards larger

displacements. The increasing uncertainty of the measurement towards larger displacements can be explained by the decreasing sensitivity of the sensor assembly, resulting in smaller and more focused spot images on the detector, with speckles of higher relative intensity and thus higher influence on the CoG uncertainty.

To illustrate the effects of the diffuser mechanism on the shape of the measurement spot image on the detector, Fig. 6 shows the measured detector output in the region of the spot location. In Fig. 6(a) and (b) the detector output without diffuser is shown with the intensity on the vertical axis in (a) and a top view on the x-y-plane in (b). It can be seen that the intensity is highly unevenly distributed over the illuminated pixels and clearly deviates from an ideal Gaussian intensity profile. The related speckle pattern can be observed with high intensity pixels determining the resulting CoG location of the spot in a disproportional way. When integrating the diffuser mechanism the detector outputs in Fig. 6(c) and (d) are obtained. The spot image shows an almost normal intensity distribution, with only a single pixel with higher intensity. The maximum intensity is a factor two smaller than without diffuser, leading to a more even illumination of the pixels of the spot image and a reduced influence on the uncertainty of the CoG location.

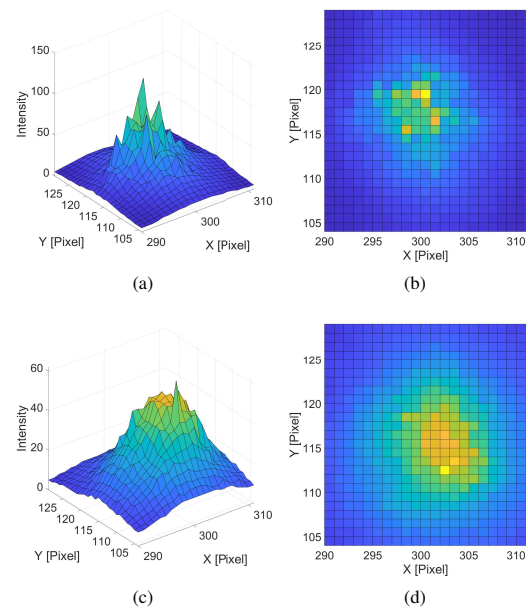


Fig. 6. Imaged measurement spots on the detector. (a) and (b) show the part of the detector with the imaged measurement spot, which significantly deviates from a Gaussian intensity profile due to speckle effects. (c) and (d) show the smoothed measurement spot with diffuser and more normally distributed intensity values.

Assessing finally the uncertainty reduction in the actual measurement due to the integration of the diffuser mechanism, Fig. 7 compares the graphs of the standard deviation of 50

measurements at each target displacement for the setup with and without diffuser. It can clearly be seen that while the uncertainty of the measurement without diffuser increases gradually towards larger displacements, as discussed previously, the uncertainty of the measurement with diffuser stays almost constant around  $15 \mu\text{m}$  over the entire measurement range. This equals a significant reduction of the resulting speckle-induced measurement uncertainty of up to 63%, as compared to the setup without diffuser.

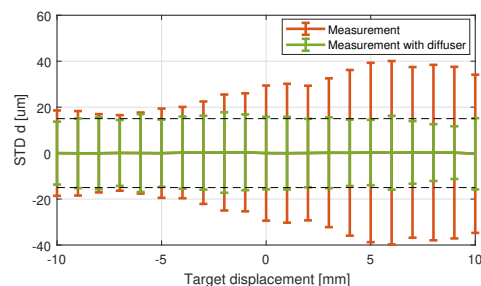


Fig. 7. Measurement uncertainty with and without diffuser. The standard deviations of respectively 50 measurement results at each displacement are shown. While the uncertainty without diffuser increases by a factor of two over the measurement range, it stays almost constant around  $15 \mu\text{m}$  with diffuser.

In summary it is shown that the simulation method can be used to accurately estimate the resulting speckle-induced uncertainty of laser-triangulation sensor assemblies and that by integrating a diffuser for speckle reduction the speckle-induced uncertainty can be reduced by up to 63%.

## V. CONCLUSION

This paper presents a method for the accurate simulation of the laser speckle-induced measurement uncertainty in the design of laser-triangulation sensor assemblies. For this purpose the simulation method integrates the stochastic nature of laser speckles with the deterministic properties of ray tracing simulations, enabling it to capture also stochastic in addition to deterministic sensor properties. To demonstrate the methods flexibility and investigate the influence of the triangulation angle on the resulting speckle-induced uncertainty, three sensor geometries with triangulation angles of  $16^\circ$ ,  $33^\circ$  and  $66^\circ$  are designed and simulated. The simulations show that the speckle-induced uncertainty varies over the entire measurement range, particularly for smaller angles, with the average uncertainty decreasing from 0.26% to 0.2% of the measurement range, if the triangulation angle is increased from  $16^\circ$  to  $66^\circ$ . To validate the accuracy of the simulation method and its results, an experimental setup with a triangulation angle of  $33^\circ$  is constructed and evaluated. The uncertainty measurements show good agreement with the simulated values, both resulting in an average standard deviation of the CoG of about  $30 \mu\text{m}$ . To reduce the impact of speckles on the measurement uncertainty, a diffuser mechanism is integrated into the optical path before the focusing

lens capable of reducing the speckle-induced measurement uncertainty by up to 63%.

Future work is concerned with integrating the speckle reduction effect into the simulation environment.

## ACKNOWLEDGMENT

The financial support by the Christian Doppler Research Association, the Austrian Federal Ministry for Digital and Economic Affairs, the National Foundation for Research, Technology and Development, Micro-Epsilon Messtechnik GmbH & Co. KG and Atensor Engineering and Technology Systems GmbH is gratefully acknowledged.

## REFERENCES

- [1] W. Gao, H. Haitjema, F. Fang, R. Leach, C. Cheung, E. Savio, and J.-M. Linares, "On-machine and in-process surface metrology for precision manufacturing," *CIRP Annals*, vol. 68, no. 2, pp. 843–866, 2019.
- [2] M. Grasso and B. M. Colosimo, "Process defects and in situ monitoring methods in metal powder bed fusion: a review," *Measurement Science and Technology*, vol. 28, no. 4, p. 044005, 2017.
- [3] H. Schwenke, U. Neuschaefer-Rube, T. Pfeifer, and H. Kunzmann, "Optical methods for dimensional metrology in production engineering," *CIRP Manufacturing Technology*, vol. 51, no. 2, pp. 685–699, 2002.
- [4] F. Blais, "Review of 20 years of range sensor development," *Journal of Electronic Imaging*, vol. 13, no. 1, 2004.
- [5] C. P. Keferstein and W. Dutschke, *Fertigungsmesstechnik*. Wiesbaden: Springer Vieweg, 2010.
- [6] F. J. Brosted, J. J. Aguilar, D. Guillomía, and J. Santolaria, "3d geometrical inspection of complex geometry parts using a novel laser triangulation sensor and a robot," *Sensors*, vol. 11, no. 1, pp. 90–110, 2010.
- [7] R. G. Dorsch, G. Häusler, and J. M. Herrmann, "Laser triangulation: fundamental uncertainty in distance measurement," *Applied optics*, vol. 33, no. 7, pp. 1306–1314, 1994.
- [8] R. Leach, *Optical measurement of surface topography*. Springer, Berlin Heidelberg, 2011, vol. 14.
- [9] F. J. W. Goodman, "Some fundamental properties of speckle," *JOSA*, vol. 66, no. 11, pp. 1145–1150, 1976.
- [10] T. Mueller, A. Poesch, and E. Reithmeier, "Measurement uncertainty of microscopic laser triangulation on technical surfaces," *Microscopy and Microanalysis*, vol. 21, no. 6, pp. 1443–1454, 2015.
- [11] M. Mohammadkaji and et al., "A framework for uncertainty propagation in 3d shape measurement using laser triangulation," *IEEE International Instrumentation and Measurement Technology Conference Proceedings*, pp. 1–6, 2016.
- [12] —, "Sensor-realistic simulations for evaluation and planning of optical measurement systems with an application to laser triangulation," *IEEE Sensors Journal*, vol. 20, no. 10, pp. 5336–5349, 2020.
- [13] S. Ibaraki, Y. Kitagawa, Y. Kimura, and S. Nishikawa, "On the limitation of dual-view triangulation in reducing the measurement error induced by the speckle noise in scanning operations," *Journal of Adv Man Tech*, vol. 88, no. 1-4, pp. 731–737, 2017.
- [14] E. Csencsics, T. Wolf, and G. Schitter, "Speckle simulation tool for the design of laser-based displacement sensors," in *Optical Measurement Systems for Industrial Inspection XII*, vol. 11782. International Society for Optics and Photonics, 2021, p. 117820G.
- [15] Y. Petrov. (2021) Optometrika - matlab library. Mathworks website: <https://de.mathworks.com/matlabcentral/fileexchange/45355-optometrika>. [Online]. Available: <https://github.com/caiuspetronius/Optometrika>
- [16] T. Yoshizawa, *Handbook of optical metrology: Principles and Applications*. CRC Press, 2017.
- [17] J. Schlarp, E. Csencsics, and G. Schitter, "Design and evaluation of an integrated scanning laser triangulation sensor," *Mechatronics*, vol. 72, p. 102453, 2020.
- [18] T. Stangner, H. Zhang, T. Dahlberg, K. Wiklund, and M. Andersson, "Step-by-step guide to reduce spatial coherence of laser light using a rotating ground glass diffusor," *Applied optics*, vol. 56, no. 19, pp. 5427–5435, 2017.